

# Optimization of lag phase shapes the evolution of a bacterial enzyme

Bharat V. Adkar<sup>1</sup>, Michael Manhart<sup>1</sup>, Sanchari Bhattacharyya<sup>1</sup>, Jian Tian<sup>1,2</sup>, Michael Musharbash<sup>1</sup> and Eugene I. Shakhnovich<sup>1\*</sup>

**Mutations provide the variation that drives evolution, yet their effects on fitness remain poorly understood. Here we explore how mutations in the essential enzyme adenylate kinase (Adk) of *Escherichia coli* affect multiple phases of population growth. We introduce a biophysical fitness landscape for these phases, showing how they depend on molecular and cellular properties of Adk. We find that Adk catalytic capacity in the cell (the product of activity and abundance) is the major determinant of mutational fitness effects. We show that bacterial lag times are at a well-defined optimum with respect to Adk's catalytic capacity, while exponential growth rates are only weakly affected by variation in Adk. Direct pairwise competitions between strains show how environmental conditions modulate the outcome of a competition where growth rates and lag times have a tradeoff, shedding light on the multidimensional nature of fitness and its importance in the evolutionary optimization of enzymes.**

Random mutagenesis is often used to assess the distribution of fitness effects in simple experimental models such as propagating viruses and microbes evolving under antibiotic stress<sup>1,2</sup>. However, the enormous size of sequence space severely constrains how much of the fitness landscape over genotypes can be explored this way. Mechanistic and predictive insights from these experiments are further limited by a lack of knowledge of the molecular effects of mutations. Instead, a more targeted experimental approach relies on the concept of a biophysical fitness landscape, in which fitness effects of mutations are mapped through their effects on molecular traits of the mutated proteins. In this approach, biophysically rational genetic variation is introduced on the chromosome, and the molecular and phenotypic effects of that variation are analysed concurrently<sup>3–6</sup>. By mapping fitness effects to variation of molecular properties rather than directly to sequences of mutated proteins, we can dramatically reduce the dimensionality of the genotype-to-phenotype mapping. The underlying hypothesis is that variation in a small number of properly selected molecular traits of mutated proteins can explain most of the resulting mutational variation in fitness, and that the relationship between these molecular traits and fitness is smooth and continuous. Several recent studies have supported this approach<sup>5–7</sup>.

The relationship between sequence variation and fitness is further confounded by the fact that multiple life-history traits contribute to fitness<sup>8</sup>, and the relative importance of these traits to the long-term evolutionary fate of a mutation may be highly dependent on environmental and ecological conditions. While multicellular organisms are generally described by a large number of traits (for example, viability at various life phases, mating success, fecundity, and so on), unicellular microorganisms such as bacteria and yeast are described by relatively fewer components of fitness, such as the time in lag phase, the exponential growth rate, and the overall yield at saturation. However, even for the relatively simpler cases of unicellular organisms (the focus of the present study), all these phases of growth contribute towards the outcome when in competition for limited resources, and hence determine fitness<sup>3,9</sup>. The relative importance of these different phases of bacterial growth

in sculpting the fitness landscape depends on the conditions of growth and competition<sup>10–12</sup>.

Overall, the challenge in quantitatively characterizing the biophysical fitness landscape is twofold: understanding fitness in terms of contributions from different phases of growth, and linking each of these components to an intermediate phenotype (molecular and cellular traits) that in turn are connected to their genotypes. In this work, we address both challenges by introducing biophysically rational genetic variation in the *adk* locus that encodes the essential *E. coli* enzyme adenylate kinase (Adk), and projecting the ensuing variations of fitness effects (phenotypic components such as growth rate and lag time) onto the biophysical traits of Adk. We find that a unique combination of molecular and cellular traits of Adk—the product of intracellular abundance and catalytic activity, which we term catalytic capacity—provides a useful predictor of fitness effects across the full range of phenotypic variation. Furthermore, we find that the length of the lag phase is more sensitive to variation in Adk catalytic capacity than is the exponential growth rate, so that the lag phase of the wild-type *E. coli* appears to be optimal with respect to variation in Adk catalytic capacity.

## Results

**Biophysical properties of Adk mutants.** Destabilizing mutations have been shown to cause a drop in intracellular protein abundance, mostly through a decrease in the folded fraction of the protein<sup>3</sup>. Hence, in order to sample a broad range of molecular and cellular traits of Adk protein below the wild-type levels, we chose a set of 21 missense mutations at 6 different positions of *adk* (Fig. 1 and Supplementary Table 1). We selected residues such that their accessible surface area was less than 10% and they were at least 6 Å away from the catalytically active sites of Adk, so that mutations at these residues were likely to destabilize the protein<sup>13</sup>. For most mutants, we chose amino acid mutations that appeared only at low frequency in an alignment of 895 homologous sequences of Adk. As intended, the purified mutant proteins were destabilized over a wide range (~17 °C in terms of  $T_m$ , and ~7.5 kcal mol<sup>-1</sup> in terms of folding  $\Delta G$ ) (Fig. 1b, Supplementary Table 1 and Supplementary Figs 1 and 2).

<sup>1</sup>Department of Chemistry and Chemical Biology, Harvard University, 12 Oxford Street, Cambridge, Massachusetts 02138, USA. <sup>2</sup>Biotechnology Research Institute, Chinese Academy of Agricultural Sciences, 12 Zhongguancun South Street, Beijing, 100081, China. \*e-mail: shakhnovich@chemistry.harvard.edu

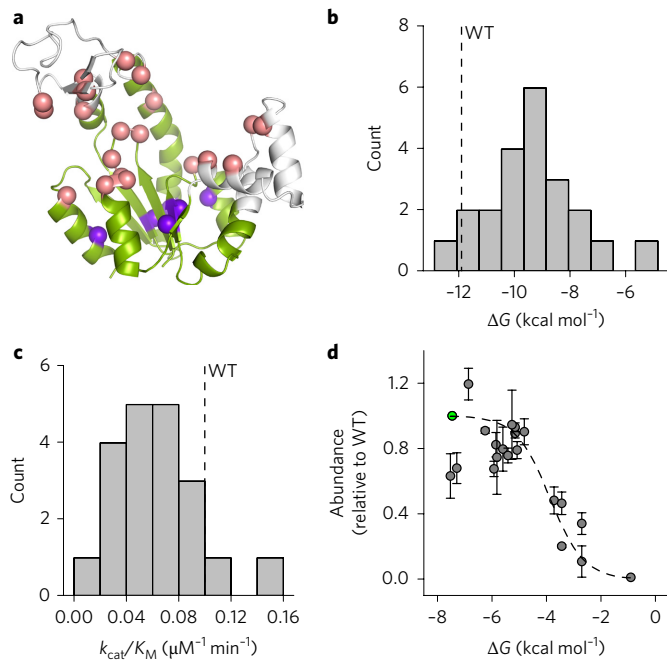


**Figure 1 | Biophysical and intracellular properties of Adk.** **a**, Crystal structure of adenylate kinase from *E. coli* (Protein Data Bank ID: 4AKE<sup>30</sup>). The Core domain is coloured in green, while the LID and NMP domains are shown in white. The C<sub>α</sub> atoms of active-site residues are shown in pink, and the blue spheres represent the C<sub>α</sub> atoms of the six buried positions that were mutated in this study. **b**, Histogram showing the distribution of folding free energies for all mutant proteins, as determined by isothermal urea denaturation at 25 °C. The stability of WT is marked by a dashed line. **c**, Histogram of the catalytic activity parameter  $k_{\text{cat}}/K_M$  for all mutants. The dashed line indicates the WT value. **d**, Total intracellular abundance of mutant Adk proteins as a function of  $\Delta G$  at 37 °C. The abundances are normalized to the WT value (green circle). Each data point represents the mean and error bars are the standard deviation over two experiments. The dashed line represents the fit to the Boltzmann distribution function described in equation (1), where  $k_B$  was 1.987 cal mol<sup>-1</sup> K<sup>-1</sup>. See related Supplementary Figs 1–5 and Supplementary Table 1.

In only one case (L209I) did we change the *E. coli* sequence to the consensus amino acid at that position, and we found that it in fact stabilized the protein by  $\sim 1$  kcal mol<sup>-1</sup> (Supplementary Table 1). Although most of the Adk mutants were less stable than the wild type, they nevertheless existed predominantly as monomers in solution (Supplementary Fig. 3). However, several mutations in one position—V106H, V106N and V106W—did have significant fractions of proteins present in higher oligomeric forms, in addition to the predominant monomeric species (Supplementary Fig. 3). These proteins bound 4,4'-dianilino-1,1'-binaphthyl-5,5'-disulfonate (Bis-ANS) dye to a higher degree compared with the rest of the mutants (Supplementary Fig. 4), indicating the presence of possible molten globule states in solution<sup>14</sup>. The proteostat dye that reports on protein aggregation<sup>4,15</sup> also bound these mutants more strongly compared with others (Supplementary Fig. 4), clearly indicating a higher fraction of aggregated species. The catalytic efficiency ( $k_{\text{cat}}/K_M$ ) of the mutant Adk proteins was distributed broadly, with most mutants showing a lower activity than *E. coli* WT (Fig. 1c, Supplementary Table 1 and Supplementary Fig. 5).

**Intracellular abundance of Adk follows prediction from Boltzmann distribution.** We then incorporated each of the 21 *adk* mutations one at a time into the *E. coli* chromosome using a genome-editing approach based on homologous recombination<sup>3,4</sup>. We measured

the total intracellular abundance of WT and mutant Adk proteins using a quantitative western blot (Supplementary Table 2). The sigmoidal dependence of total intracellular Adk abundance on folding stability ( $\Delta G$ ) (Fig. 1d) is well described by the Boltzmann distribution for two-state unfolding of proteins:

$$P_F = \frac{1}{1 + \exp(\beta\Delta G)} \quad (1)$$

where  $P_F$  is the fraction of folded molecules in the ensemble of intracellular Adk and  $\beta = 1/k_B T$ , with Boltzmann constant  $k_B$  and growth temperature  $T$ . The total measured abundance of a protein is its amount in the cytoplasm at steady state, achieved by a balance between production and degradation. Since Adk is expressed from a constitutive promoter in the cells, it is generally safe to assume that the rates of production of all mutants are similar. Under this assumption, the sigmoidal dependence of abundance on stability clearly indicates that the unfolded protein is degraded in the active medium of the cytoplasm.

**Mutations in Adk affect lag times more than exponential growth rates.** Mutations in Adk affect both intracellular abundance (via folding stability) and catalytic activity of the protein. Flux dynamics theory predicts, and experiments have confirmed, that the key enzymatic parameter determining the flux through an enzymatic reaction chain is the quantity that we call catalytic capacity, defined as the product of intracellular abundance and enzymatic efficiency  $k_{\text{cat}}/K_M$ <sup>5,6,16</sup>. Here we determine how two key components of bacterial growth—the exponential growth rate and the lag time (Fig. 2a)—depend on the total catalytic capacity of Adk in *E. coli* cells (Fig. 2b,c; also see Methods and Supplementary Figs 6–8 for estimations of growth parameters). We find that while only 3 out of 21 strains show a drop in growth rate greater than 5% of the WT, 17 strains show an increase in lag time for a similar change over the WT value (Supplementary Table 2). This suggests that the mutations in Adk affect the lag phase more significantly than the exponential growth phase. One way in which longer lag times can be observed is when a greater proportion of cells that come out of stationary phase are simply nonviable, as described in a recent study<sup>17</sup>. However, this appears not to be the major cause in our case, as lag times are fairly consistent across replicates (error bars in Fig. 2c) and do not negatively correlate with the number of viable cells (Supplementary Fig. 9). We also find that the variation in total catalytic capacity of Adk correlates better with the variation in lag times (Spearman's rank correlation  $\rho = -0.44$ ,  $p = 0.057$ ) than with the variation in growth rates (Spearman's rank correlation  $\rho = -0.08$ ,  $p = 0.737$ ) (Supplementary Fig. 10). The variation in lag times is also better explained by the variation in catalytic capacity than with any of the Adk properties separately (stability, abundance or activity) (Supplementary Fig. 10). Surprisingly, growth rate appears to tolerate a rather large drop in catalytic capacity of Adk, while lag time does not. While the nonlinear relationship between catalytic capacity and lag times (Fig. 2c) makes it difficult to determine exactly how much mutational variation in lag times is quantitatively explained by variation in catalytic capacity, the model-independent Spearman rank correlation indicates that catalytic capacity predicts 20–25% of the rank variation in lag times, depending on the method of lag time estimation (see Methods).

**WT *E. coli* is positioned at the cusp of the biophysical fitness landscape for lag time.** Since almost all the designed mutants were destabilizing and therefore have lower catalytic capacity than *E. coli* WT, they only provide sampling in the lower range of catalytic capacity. In studies so far, no evidence exists for changes in intracellular protein abundance for stabilizing mutations. Hence, to determine the dependence of growth rate and lag time on catalytic capacity above WT levels, we overexpressed WT Adk from a pBAD plasmid

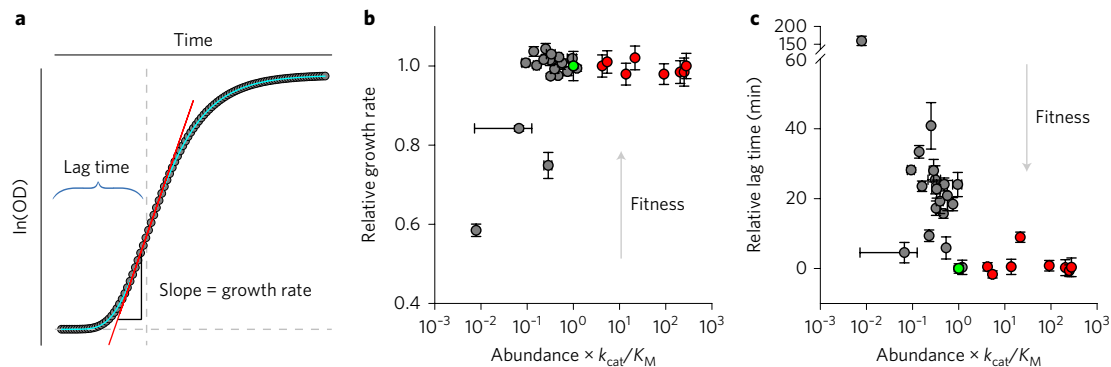


**Figure 2 | Traits of population growth.** **a**, Schematic of estimation of lag time and growth rate. The representative data points (solid grey circles) were plotted as  $\ln(\text{OD})$  versus time, and were fitted to a four-parameter Gompertz function (equation (2)) (cyan line). The red line is a tangent at the inflection point of the function. The slope of the tangent is considered as the growth rate ( $\mu$ ) and the time required to reach the maximum growth rate or the inflection point is taken as the lag time ( $\lambda$ ) (vertical dashed line). **b,c**, Relative growth rate ( $\mu/\mu_{\text{WT}}$ ) (**b**) and relative lag time ( $\lambda - \lambda_{\text{WT}}$ ) (**c**) as functions of catalytic capacity, which is defined as  $\text{abundance} \times k_{\text{cat}}/K_M$  (using experimentally measured abundance and activity values). The mutant data is shown in grey circles, whereas red circles represent the BW27783 strain with varying degrees of overexpression of WT Adk from a pBAD plasmid. Data for WT is shown in green. The data points represent mean and error bars represent s.e.m. of parameters derived from growth curves of 2–3 bacterial colonies (biological replicates). See Supplementary Figs 6–11 and Supplementary Tables 2 and 3. The direction of increasing fitness is also indicated.

(see Supplementary Methods). We observed no significant change in either growth rate or lag time at higher than endogenous catalytic capacity (Fig. 2b,c, Supplementary Fig. 8 and Supplementary Table 3). This means that while the growth rate appears to be insensitive to large changes in Adk catalytic capacity both below and above the WT level, WT catalytic capacity appears to be situated at the threshold of optimizing lag time.

Next, we attempted to quantitatively compare the position of WT on these two fitness landscapes. To that end, we used a simple reciprocal Michaelis–Menten-like function to fit the relative growth times (growth time,  $\tau$ , is reciprocal of growth rate,  $\mu$ ) and lag times (Supplementary Fig. 11; also see equation (3) and Methods). The fitting parameter  $b$ , which characterizes the onset of curvature on the landscape (analogous to  $K_M$  in the Michaelis–Menten equation for enzymatic rate) reports the proximity of WT to the cusp on the landscape (see Methods); it was  $0.006 \pm 0.003$  for growth time and  $0.019 \pm 0.004$  for lag time, as compared to normalized catalytic capacity of 1 for WT. This shows that WT is situated closer to the cusp in terms of lag time as compared to growth time (equivalently, growth rate).

**A computational model demonstrates advantage of shorter lag at low carrying capacity.** This data highlights the pleiotropic effects of mutations on different phases of bacterial population growth, which raises the question of how pleiotropy shapes the evolutionary fate of a mutation. We explore this issue by considering the outcome of binary competitions between strains<sup>18</sup>. We first simulated binary competitions over a wide range of growth rates and lag times in media conditions that allow for either 5-fold or 500-fold increases over the initial population at carrying capacity, which is analogous to low and high carrying capacity conditions (Fig. 3a) (see Methods). We found that there is a significant tradeoff between lag times and growth rates in determining the winners of binary competitions, with lag playing a more important role at low carrying capacity (Fig. 3a)—implying that beneficial lag provides a greater fitness advantage under strongly nutrient-limiting conditions.

**Experimental evidence to demonstrate advantage of shorter lag at low carrying capacity.** To realize varying nutrient conditions in binary competition experiments, we explored the growth of *E. coli* over a range of glucose concentrations, mimicking the variation of carrying capacity in simulations, and found that only the carrying capacities (the fold excess over the initial population) are proportional to glucose concentration, with minimal effects on lag time and

growth rate (Fig. 4). This suggests that observing the outcome of the competition at different time snapshots in a nutrient-rich medium is equivalent to running the competition at different glucose concentrations (carrying capacities). To evaluate the predictions from simulations, we carried out two sets of binary competition experiments based on the overall distribution of growth rates and lag times (Fig. 3b). First, we selected strains exhibiting a tradeoff between growth rate ( $\mu$ ) and lag time ( $\lambda$ ) ( $\mu_1 > \mu_2$  and  $\lambda_1 > \lambda_2$ ) (inset of Fig. 5b). Second, we tested competition between strains that differ in their lag times but have nearly indistinguishable growth rates ( $\mu_1 \approx \mu_2$  and  $\lambda_1 > \lambda_2$ ) (inset of Fig. 5c). In all cases, a strain with shorter lag time is expected to dominate at lower carrying capacity conditions (corresponding to the competition outcome at early time points where the

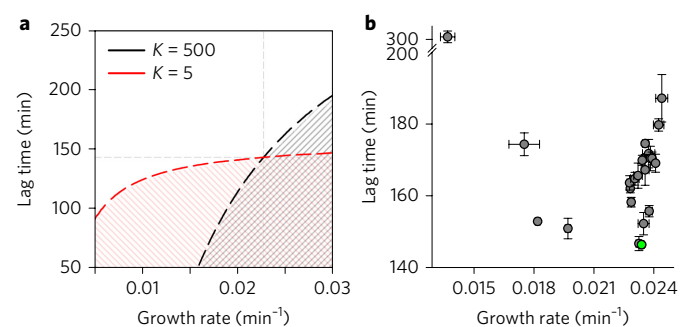


**Figure 3 | Binary growth competition.** **a**, The growth of individual strains was modelled as per the Gompertz equation (equation (2)). The growth parameters for strain 1 were fixed to those obtained for WT Adk (dashed grey lines) while those for strain 2 were generated randomly over a wide range of growth rates (0.005 to 0.030  $\text{min}^{-1}$ ) and lag times (50 to 250 min). The contour plot shows the fraction of strain 1 (WT) at saturation when the competition is carried out under two different conditions of fold increase in growth over initial population. The red and black dashed lines indicate the neutrality regions where both strains have equal proportions at saturation. The areas below the neutrality lines (filled with solid lines) represent the parameter space where strain 2 wins the competition (fraction of strain 2  $> 0.5$ ). **b**, Scatter plot of measured growth rate ( $\mu$ ) versus lag time ( $\lambda$ ). The data points represent the mean and error bars the s.e.m. of parameters derived from 2–3 bacterial colonies (Supplementary Table 2). The growth rate and lag time appear to be statistically independent of each other across the Adk mutant strains (Spearman's  $\rho = 0.31$ ,  $p = 0.15$ ).

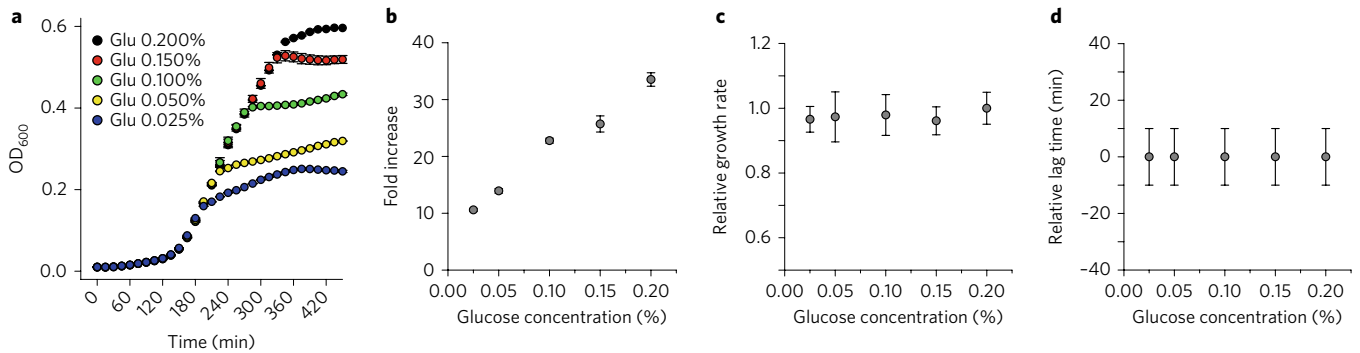


**Figure 4 | Growth curves at various nutrient concentrations.** **a–d**, Growth curves of strains with WT Adk obtained under varying glucose concentrations in supplemented M9 medium (**a**). The fitted growth curve parameters are shown as functions of glucose concentration: fold increase over initial population at saturation ( $K$ ) as derived from a Gompertz fit (**b**), relative growth rate ( $\mu/\mu_{0.2}$ ) (**c**), and relative lag time ( $\lambda - \lambda_{0.2}$ ) (**d**). The growth rates and lag times are estimated from analysis of growth curve derivatives and are normalized relative to the respective values at 0.2% glucose concentration.

fold increase over initial population is low); however, this advantage would be lost at later time points if its growth rate is lower than that of the competing strain (Fig. 5a). In the second scenario, the advantage due to short lag is expected to persist even at high carrying capacity conditions because the growth rates of the competing strains do not differ. We estimated the relative proportions of the two strains by a quantitative PCR (qPCR)-based mismatch amplification mutation assay (MAMA) approach<sup>19</sup> (see Methods and Supplementary Fig. 12). As expected in the first scenario, L083F and V106H dominated at earlier time points when competed against A093I and L209I, respectively, due to their shorter lag times ( $\lambda_{L083F} < \lambda_{A093I}$  and  $\lambda_{V106H} < \lambda_{L209I}$ ) (Fig. 5b). Eventually their fractions dropped below 0.5 at later time points (equivalent to high carrying capacity), when the growth rates determine the competition output ( $\mu_{L083F} < \mu_{A093I}$  and  $\mu_{V106H} < \mu_{L209I}$ ) (Fig. 5b). Similarly, for the second scenario, despite having similar growth rates ( $\mu_{WT} \approx \mu_{Y182V} \approx \mu_{L209A}$ ), the fraction of WT was always maintained above 0.5 as it spends a shorter time in the lag phase compared to Y182V and L209A (Fig. 5c). The early advantage of WT due to its shorter lag phase determined the competition fitness throughout the whole growth cycle.

## Discussion

A complete mapping of mutational fitness effects would require sampling a practically infinite number of mutations—an impossible proposition. Instead, we can project fitness onto a fairly small number of molecular properties of proteins<sup>5–7,20</sup>. Within this paradigm, the identity of a particular mutation does not matter as much as its effect on essential biochemical and biophysical properties of the proteins in question. Our 21 engineered mutations in Adk, along with the overexpression data, allow us to outline the biophysical fitness landscape, covering a wide range of variation of the physical parameters of the Adk protein. This data shows that we can collapse several molecular phenotypes into a single effective molecular trait—the product of protein abundance and activity  $k_{cat}/K_M$  (catalytic capacity)—which quantitatively determines the biophysical fitness landscape (Fig. 2b,c). That is, Fig. 2 indicates that phenotypic traits exhibit (within uncertainties of experimental measurements) a monotonic dependence on a single molecular trait, catalytic capacity, thereby making the corresponding biophysical fitness landscape ‘smooth’ and qualitatively predictive. Indeed, Adk catalytic capacity explains a significant fraction of rank variation in lag times, validating the use of a low-dimensional biophysical fitness landscape for semi-quantitative mapping of fitness effects.

These results illustrate how the evolutionary endpoint of molecular traits may depend fundamentally on the multidimensional nature of fitness, with the relative importance of different components of fitness depending on the environment and lifestyle of the

organism. It has been argued that endogenous molecular traits are established as a result of mutation–selection balance<sup>21</sup>, with the final outcome depending on the relative strengths of selection and genetic drift as determined by the population structure<sup>22,23</sup>. Here we encounter a more complex situation where mutations in the essential enzyme Adk change multiple fitness components. In this case, the mutation–selection balance apparently resulted in disparate outcomes for the two fitness components with respect to the molecular trait, placing lag time at the cusp while keeping the exponential growth rate farther within the plateau region of its respective biophysical fitness landscape. Such an outcome may reflect different strengths of selection on growth and lag. The relative strength of selection on these fitness components depends crucially on the environmental conditions (such as nutrient availability and so on)<sup>24</sup>. Our studies of binary competitions (Figs 3 and 5) highlight this scenario by showing how the environmental parameter of carrying capacity can determine winners and losers in evolutionary dynamics. Although the lag time of a population can depend not only on the environment but also on the population’s specific history (for example, how long it was previously in stationary phase), the fundamental role of Adk in metabolism suggests that its effects on lag time are likely to be common across conditions and histories. The deep connection between the ecological history of species and optimization of biophysical traits of their proteins is a subject for future studies.

Much of our current understanding of microbial cultures and fitness comes from experiments done in the laboratory, where strains are typically grown under a large supply of nutrients. The situation might be very different in the wild, however, where bacteria and other microbes have to survive under harsh conditions of nutrient starvation, extreme temperature, and other environmental stresses<sup>25–27</sup>. For example, *E. coli* is the predominant facultative anaerobe in the gastrointestinal tract<sup>28</sup>, which allows it to thrive in fluctuating environments of differing oxygen concentrations (such as in the small versus the large intestine). In these circumstances, organisms are likely to spend only a minute fraction of their life cycle in the exponential growth phase, while undergoing many cycles of lag–growth–saturation as new resources become available and old ones are exhausted. It is therefore intuitive to expect that there has been strong selection in favour of organisms that can not only divide rapidly during exponential growth, but that can also wake up quickly from their lag phase and respond to newly available resources. Our study demonstrates how this selection may shape individual molecular traits.

This work highlights the relationship between various components of fitness and the molecular properties of modern enzymes—the endpoint of evolutionary selection. An interesting question

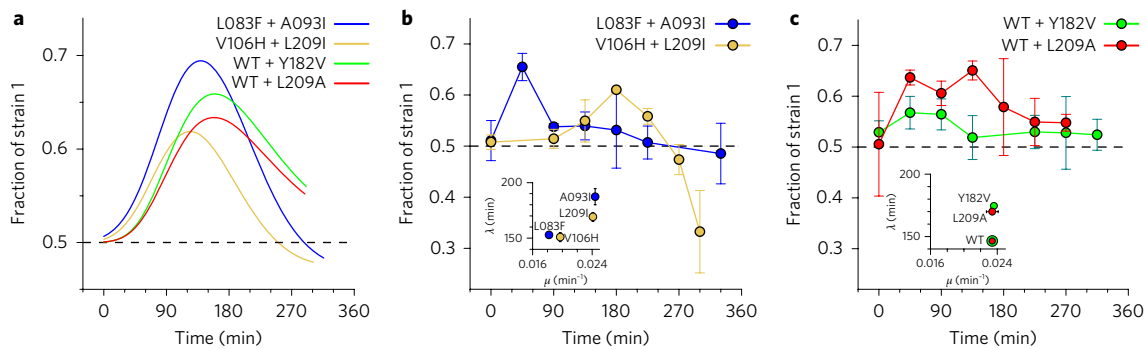


**Figure 5 | Tradeoffs between lag and exponential growth in binary competitions.** **a**, Fraction of the first strain as a function of time in simulated binary competitions. We modelled the growth of each strain using the Gompertz four-parameter equation (equation (2)) with experimentally measured growth rate and lag time values. The initial OD for individual strains was assumed to be 0.006 at the start of competition, and growth was assumed to saturate at an OD of 0.6. Despite having similar growth rates, the fraction of WT in WT + L209A and WT + Y182V competitions was always above 0.5 owing to the advantage it gained due to shorter lag time (scenario 2 in the main text). L083F and V106H dominate at earlier time points where fold increase in growth over initial population is low (equivalent to low carrying capacities) due to their short lag times compared to their respective competitors. However, at longer times (high carrying capacities), the advantage due to lag is lost due to their lower growth rates. **b,c**, Experimental validations of the predictions in **a** using a qPCR-based mismatch amplification mutation assay (MAMA). The fraction of competing strains was estimated using equation (4). The data points are mean and error bars represent standard deviation of two measurements. See Supplementary Fig. 12. The growth rates and lag times for the competing pairs are shown in insets.

that is beyond the scope of this current work is how modern variants emerged in evolutionary dynamics. To that end, mapping reconstructed ancestral species onto the biophysical fitness landscape of Adk (and other enzymes) appears to be a promising direction for future research.

## Methods

**Selection of mutations.** Mutations at relatively buried positions generally result in decreased stability and lower fitness<sup>13,29</sup>. Hence we selected the sites for mutagenesis with side-chain accessibility of less than 10%. In addition, the selected sites were also away from the active-site residues, or active-site contacting residues, and a minimum of 6 Å away from the inhibitor Ap5A binding sites (PDB ID: 1AKE). The structure of Adk is divided into three domains: LID (residues 118–160), NMP (residues 30–67), and Core (residues 1–29, 68–117, and 161–214). We define the active-site residues as those whose accessible surface area changes by at least 5 Å<sup>2</sup> in the presence of the inhibitor Ap5A. A similar criterion was used to define the residues contacting the active site. Altogether 4 residues from the LID domain, 3 from the NMP domain, and 28 from the Core domain satisfy these criteria. Of the 28 sites from the Core domain, we randomly chose 6 to mutate. We chose the identities of the mutations to span various sizes of the side chains and a range of conservation. We derived the conservation from the multiple sequence alignment of 895 sequences for Adk collated from the ExPASy database (as of November 2012).

**Generation of mutant strains.** We generated the strains with WT and mutant *adk* with chloramphenicol- and kanamycin-resistance genes on either end of the *adk* gene using a genome editing approach described previously<sup>3</sup>. Since the *adk* gene is flanked by two repeat regions (REPT44 and REPT45) on the WT chromosome, we extended the homology required for recombination up to the middle of the adjacent genes.

**Growth curve measurements and media conditions.** WT and mutant strains were grown overnight at 30 °C from single colonies in a supplemented M9 medium (0.2% glucose, 1 mM MgSO<sub>4</sub>, 0.1% casamino acids, and 0.5 μg ml<sup>-1</sup> thiamine). OD<sub>600</sub> was measured for all the strains and the cultures were then normalized to whichever had the lowest OD. The normalized cultures were diluted 1:100 in fresh supplemented M9 media and the growth curves were monitored in triplicates using Bioscreen C at 37 °C. We derived the growth parameters by fitting ln(OD) versus time with the four-parameter Gompertz function (see below). The error in replicates was found to be 2–3% on average, and it did not improve significantly upon increasing the number of replicates.

**Fitting growth data and estimation of growth parameters.** In our study, we define lag time ( $\lambda$ ) as the time required to achieve the maximum growth rate ( $\mu$ ) (Fig. 2a). Growth time ( $\tau$ ) was defined as reciprocal of growth rate  $\mu$ . Since it has the same units as lag time, it is more convenient to use for the statistical analysis and data fitting (Supplementary Fig. 11).

We used two different methods to infer these parameters: (A) direct analysis of growth curve derivatives, and (B) fits to the Gompertz function (Supplementary Fig. 6).

In method A, we took the growth rate as the maximum value of the derivative

$$\frac{\ln(\text{OD}(t)/\text{OD}(t-\Delta t))}{\Delta t}$$

where  $\Delta t$  is 15 minutes. The lag time was then the earliest time at which this maximum growth rate was achieved.

For method B, we used the following four-parameter Gompertz function to fit ln(OD) versus time plots:

$$\ln(\text{OD}) = \ln(\text{OD}_0) + \ln(K) \exp\left[-\exp\left(-\frac{t-\lambda}{b}\right)\right] \quad (2)$$

where  $K$  is the fold increase over initial population at saturation, the maximum growth rate is  $\mu = \ln(K)/(b \exp(1))$ , and the lag time  $\lambda$  is the time taken to achieve the maximum growth rate.

For both methods, we considered only data points with OD<sub>600</sub> ≥ 0.02. The instantaneous derivatives of all growth curves show the presence of a distinct peak at OD<sub>600</sub> values greater than 0.02 (Supplementary Fig. 6), indicating monoauxic growth and also asserting that the derived growth parameters are unaffected due to ignoring the lower OD data.

The  $\mu$  and  $\lambda$  estimated from the two aforementioned methods are strongly correlated (Pearson's  $r = 0.80$ ,  $p = 1.4 \times 10^{-5}$  for  $\mu$ , and  $r = 0.71$ ,  $p = 3.0 \times 10^{-4}$  for  $\lambda$ ) (Supplementary Fig. 7). However, the uncertainty in the fitted parameters appears to be less than the uncertainty in the parameters obtained from the derivatives, which are limited by the low time resolution of the experimental data (acquired at an interval of 15 min).

The growth rate ( $\mu$ ) and lag time ( $\lambda$ ) appear to be statistically independent of each other across the Adk mutant strains (Spearman's  $\rho = 0.31$ ,  $p = 0.15$ ; Fig. 3b). Hence it is conceivable that selection can act separately on these two traits, which is further illustrated by the different fitness landscapes observed when projected onto the axis of catalytic capacity (Fig. 2b,c).

**Statistical tests for mutational variation in growth and lag phases.** We estimated the monotonic relationship between various growth traits and molecular/cellular properties of Adk mutant proteins using Spearman's rank correlation  $\rho$  (Supplementary Fig. 10). Due to the nonlinear relationship between these properties, we used the square correlation coefficient  $\rho^2$  to measure the fraction of variance of fitness component ranks explained by the variance of ranks of the molecular/cellular properties. The agreement between growth parameters derived using instantaneous derivatives and Gompertz fit were estimated by Pearson's correlation coefficient (Supplementary Fig. 7). We excluded V106N from all statistical analysis and data fitting as its lag time is ~13 s.d. away from the average lag time of all other strains.

**Quantification of the location of WT on the fitness landscapes.** A Michaelis-Menten-like elasticity curve function has been used previously<sup>5,6,16,20</sup> to fit

the dependence of growth rate on catalytic capacity. Since we are considering growth and lag times rather than rates, we use a reciprocal form of the Michaelis–Menten-like function for fitting relative growth time ( $\tau/\tau_{WT}$ ) and relative lag time ( $\lambda/\lambda_{WT}$ ) versus catalytic capacity (Supplementary Fig. 11):

$$\text{Relative growth trait} = \frac{a \times (b + \text{catalytic capacity})}{\text{catalytic capacity}} \quad (3)$$

where  $a$  is the asymptotic value of the trait for infinitely large catalytic capacity, and  $b$  is the catalytic capacity when the trait equals twice the asymptotic value (2a). Since catalytic capacity is normalized by WT,  $b$  serves as a measure of how close to the cusp the WT is on the respective landscapes. For fits in Supplementary Fig. 11, we empirically set  $a = 1$ , which enables easy comparison of parameter  $b$  for lag time and growth time plots.

**Simulation of binary competition.** We simulated the competition of two strains by using the Gompertz function (equation (2)) to model the growth of individual strains. The initial population ( $OD_0$ ) for both strains was equal, and growth ceases when  $\sum_i OD_{t,i} / \sum_i OD_{0,i} = K$ , where  $K$  is the fold increase over initial population that is allowed by the given environmental condition, analogous to its carrying capacity. We considered two different values of  $K$  (5 and 500). We set  $\mu_i$  and  $\lambda_i$  to values derived experimentally for the WT Adk strain (Supplementary Table 2), while the growth rates and lag times for the second competing strain were varied randomly across the intervals 0.005 to 0.030 min<sup>-1</sup> (for growth rate) and 50 to 300 min (for lag time).

**Binary growth competition and quantification.** The overnight cultures for individual strains were grown for 16 hours at 30 °C. These cultures were mixed in proportions of 1:1, diluted to an OD of 0.01 in fresh supplemented M9 media, and then regrown at 37 °C. The samples were drawn at different time points, and the OD was adjusted to 2.0, either by concentration or dilution. 5 µl of OD 2.0 culture was eventually diluted in 45 µl of lysis solution (QuickExtract DNA extraction solution (Epicentre)) to reach OD 0.2. Genomic DNA extracted from 50 µl of OD 0.2 culture was diluted 5,000 times and used as a template. The individual strains in the competition were differentially amplified using allele-specific primers and quantified by a qPCR-based mismatch amplification mutation assay method<sup>19</sup> using the QuantiTect SYBR Green PCR kit (Qiagen). A 150-bp-long non-mutagenic amplicon of *adk* gene was amplified as a reference to quantify total genomic DNA. The fraction of the competing strains was determined using the following equation:

$$\text{fraction} = 2^{((C_{t,ref} - C_{t,1})_{\text{competition}} - (C_{t,ref} - C_{t,1})_{\text{pure}})} \quad (4)$$

where  $C_t$  represents threshold cycle of qPCR, ‘ref’ and 1 are the PCR reactions for amplifying the reference and the first allele in competition, and ‘competition’ and ‘pure’ describe the condition of culture.

**Data availability.** All raw data for growth curves of *adk* WT and mutant strains, as well as WT overexpression in *E. coli* BW27783 strains, are included as Supplementary Dataset 1.

Received 13 August 2016; accepted 22 March 2017;  
published 28 April 2017

## References

- Sanjuan, R., Moya, A. & Elena, S. F. The distribution of fitness effects caused by single-nucleotide substitutions in an RNA virus. *Proc. Natl Acad. Sci. USA* **101**, 8396–8401 (2004).
- Bershtein, S., Segal, M., Bekerman, R., Tokuriki, N. & Tawfik, D. S. Robustness-epistasis link shapes the fitness landscape of a randomly drifting protein. *Nature* **444**, 929–932 (2006).
- Bershtein, S., Mu, W. & Shakhnovich, E. I. Soluble oligomerization provides a beneficial fitness effect on destabilizing mutations. *Proc. Natl Acad. Sci. USA* **109**, 4857–4862 (2012).
- Bershtein, S., Mu, W., Serohijos, A. W., Zhou, J. & Shakhnovich, E. I. Protein quality control acts on folding intermediates to shape the effects of mutations on organismal fitness. *Mol. Cell* **49**, 133–144 (2013).
- Bershtein, S. *et al.* Protein homeostasis imposes a barrier on functional integration of horizontally transferred genes in bacteria. *PLoS Genet.* **11**, e1005612 (2015).
- Rodrigues, J. V. *et al.* Biophysical principles predict fitness landscapes of drug resistance. *Proc. Natl Acad. Sci. USA* **113**, E1470–E1478 (2016).
- Gong, L. I., Suchard, M. A. & Bloom, J. D. Stability-mediated epistasis constrains the evolution of an influenza protein. *eLife* **2**, e00631 (2013).
- Orr, H. A. Fitness and its role in evolutionary genetics. *Nat. Rev. Genet.* **10**, 531–539 (2009).
- Elena, S. F. & Lenski, R. E. Evolution experiments with microorganisms: the dynamics and genetic bases of adaptation. *Nat. Rev. Genet.* **4**, 457–469 (2003).

- Dykhuizen, D. E. & Hartl, D. L. Selection in chemostats. *Microbiol. Rev.* **47**, 150–168 (1983).
- Biel, S. W. & Hartl, D. L. Evolution of transposons: natural selection for Tn5 in *Escherichia coli* K12. *Genetics* **103**, 581–592 (1983).
- Fridman, O., Goldberg, A., Ronin, I., Shoshitashvili, N. & Balaban, N. Q. Optimization of lag time underlies antibiotic tolerance in evolved bacterial populations. *Nature* **513**, 418–421 (2014).
- Bajaj, K., Chakrabarti, P. & Varadarajan, R. Mutagenesis-based definitions and probes of residue burial in proteins. *Proc. Natl Acad. Sci. USA* **102**, 16221–16226 (2005).
- Semisotnov, G. V. *et al.* Study of the ‘molten globule’ intermediate state in protein folding by a hydrophobic fluorescent probe. *Biopolymers* **31**, 119–128 (1991).
- Navarro, S. & Ventura, S. Fluorescent dye ProteoStat to detect and discriminate intracellular amyloid-like aggregates in *Escherichia coli*. *Biotechnol. J.* **9**, 1259–1266 (2014).
- Dykhuizen, D. E., Dean, A. M. & Hartl, D. L. Metabolic flux and fitness. *Genetics* **115**, 25–31 (1987).
- Peters, J. M. *et al.* A comprehensive, CRISPR-based functional analysis of essential genes in bacteria. *Cell* **165**, 1493–1506 (2016).
- Hegreness, M., Shoshitashvili, N., Hartl, D. & Kishony, R. An equivalence principle for the incorporation of favorable mutations in asexual populations. *Science* **311**, 1615–1617 (2006).
- Cha, R. S., Zarbl, H., Keohavong, P. & Thilly, W. G. Mismatch amplification mutation assay (MAMA): application to the c-H-ras gene. *PCR Meth. Appl.* **2**, 14–20 (1992).
- Jiang, L., Mishra, P., Hietpas, R. T., Zeldovich, K. B. & Bolon, D. N. Latent effects of Hsp90 mutants revealed at reduced expression levels. *PLoS Genet.* **9**, e1003600 (2013).
- Serohijos, A. W. & Shakhnovich, E. I. Merging molecular mechanism and evolution: theory and computation at the interface of biophysics and evolutionary population genetics. *Curr. Opin. Struct. Biol.* **26**, 84–91 (2014).
- Serohijos, A. W., Lee, S. Y. & Shakhnovich, E. I. Highly abundant proteins favor more stable 3D structures in yeast. *Biophys. J.* **104**, L1–L3 (2013).
- Hartl, D. L. & Clark, A. G. *Principles of population genetics* 4th ed. (Sinauer, 2007).
- Manhart, M., Adkar, B. V. & Shakhnovich, E. I. Tradeoffs between microbial growth phases lead to frequency-dependent and non-transitive selection. Preprint at <http://bioRxiv.org/content/early/2016/12/23/096453> (2016).
- Lambert, G., Liao, D., Vyawahare, S. & Austin, R. H. Anomalous spatial redistribution of competing bacteria under starvation conditions. *J. Bacteriol.* **193**, 1878–1883 (2011).
- Palkova, Z. Multicellular microorganisms: laboratory versus nature. *EMBO Rep.* **5**, 470–476 (2004).
- Hibbing, M. E., Fuqua, C., Parsek, M. R. & Peterson, S. B. Bacterial competition: surviving and thriving in the microbial jungle. *Nat. Rev. Microbiol.* **8**, 15–25 (2010).
- Todar, K. *Online Textbook of Bacteriology* (2015); <http://www.textbookofbacteriology.net/>
- Adkar, B. V. *et al.* Protein model discrimination using mutational sensitivity derived from deep sequencing. *Structure* **20**, 371–381 (2012).
- Muller, C. W., Schlauderer, G. J., Reinstein, J. & Schulz, G. E. Adenylate kinase motions during catalysis: an energetic counterweight balancing substrate binding. *Structure* **4**, 147–156 (1996).

## Acknowledgements

This work was supported by NIH award R01 GM068670 to E.I.S. M.Ma. was supported by NIH award F32 GM116217. We thank S. Bershtein and A. Serohijos for helpful discussions.

## Author contributions

B.V.A. and E.I.S. designed the research; B.V.A., S.B., J.T. and M.Mu. performed experiments; B.V.A., M.Ma., S.B. and E.I.S. analysed the data; B.V.A., M.Ma., S.B. and E.I.S. wrote the paper. All authors edited and approved the final version.

## Additional information

Supplementary information is available for this paper.

Reprints and permissions information is available at [www.nature.com/reprints](http://www.nature.com/reprints).

Correspondence and requests for materials should be addressed to E.I.S.

**How to cite this article:** Adkar, B. V. *et al.* Optimization of lag phase shapes the evolution of a bacterial enzyme. *Nat. Ecol. Evol.* **1**, 0149 (2017).

**Publisher's note:** Springer Nature remains neutral with regard to jurisdictional claims in published maps and institutional affiliations.

## Competing interests

The authors declare no competing financial interests.

In the format provided by the authors and unedited.

## Optimization of lag phase shapes the evolution of a bacterial enzyme

Bharat V. Adkar<sup>1</sup>, Michael Manhart<sup>1</sup>, Sanchari Bhattacharyya<sup>1</sup>, Jian Tian<sup>1,2</sup>, Michael Musharbash<sup>1</sup>, Eugene I. Shakhnovich<sup>1\*</sup>

<sup>1</sup>Department of Chemistry and Chemical Biology, Harvard University, 12 Oxford St., Cambridge, MA 02138, USA

<sup>2</sup>Biotechnology Research Institute, Chinese Academy of Agricultural Sciences, 12 Zhongguancun South Street, Beijing, 100081, China

\*Correspondence should be addressed to E.S. (shakhnovich@chemistry.harvard.edu)

This file contains:

- Supplementary Methods
- Supplementary Figures 1-12
- Supplementary Tables 1-3

## **Supplementary Methods**

### **Mutagenesis and protein purification**

Adenylate kinase (Adk) is encoded by the *adk* gene, which was cloned under the T7-*lac* promoter in pET28a(+) vector (Invitrogen) between *Nde*I and *Xho*I restriction sites. We carried out mutagenesis with a pair of 30-35 bp long, partially-complementary primers and the inverse PCR technique using KOD hot-start DNA polymerase. The mutations were centered in the complementary regions of the primers. The mutagenic plasmids were transformed in *E. coli* DH5 $\alpha$  cells for faithful propagation and storage, and in *E. coli* BL21(DE3) for protein overexpression and purification. The His-tagged proteins were purified by Ni-NTA affinity chromatography (Qiagen) and subsequently passed through a HiLoad Superdex 75 pg column (GE). The monomeric peak was collected, concentrated and eventually stored in 10 mM potassium phosphate buffer (pH 7.2). The concentration of the proteins was measured by BCA assay (ThermoScientific) with BSA as standard.

### **Biophysical characterization**

**Thermal denaturation:** We assessed the thermal stability of WT and mutant proteins by differential scanning calorimetry (nanoDSC, TA instruments) using 20  $\mu$ M of protein. The scans were carried out from 10 to 90  $^{\circ}$ C at a scan rate of 90  $^{\circ}$ C/hr. The thermodynamic parameters were derived by fitting the data to a two-state unfolding model using NanoAnalyze (TA instruments). We also carried out thermal denaturation using the melt-curve module of BioRad CFX96, with Sypro Orange dye as a probe for unfolding as described earlier<sup>1</sup>. The dye was added to the final concentration of 5 $\times$  in a 25  $\mu$ l reaction volume containing 4  $\mu$ M of protein in



10 mM potassium phosphate buffer (pH 7.2). The data were fit to a standard four-parameter sigmoidal equation to obtain apparent melting temperatures.

Urea denaturation: We carried out isothermal urea denaturation with WT and mutant proteins to assess the stability of the proteins to chemical denaturants. We incubated 5  $\mu\text{M}$  of protein for ~4 hrs at 25 °C with varying concentrations of urea (0-8 M). The urea concentrations were estimated by refractive index measurements. The denaturation was monitored by measuring the ellipticity at 222 nm using a CD spectrometer (Jasco). The melt data was fitted assuming a model of two-state unfolding with linear free energy as described earlier<sup>2,3</sup>. The m-value was fixed to 3300 cal/mol/M for fitting.

Gel filtration: We assessed the oligomeric status of purified proteins by gel filtration using 50  $\mu\text{g}$  of protein on sephadex 75 analytical columns.

ANS and proteostat binding: We used 12  $\mu\text{M}$  of bisANS for assessing binding to 2  $\mu\text{M}$  of protein in 10 mM potassium phosphate buffer (pH 7.2). The excitation and emission wavelengths were set to 395 nm and 490 nm, respectively. 2  $\mu\text{M}$  of protein was incubated with 3.5 mM of the proteostat dye in 1 $\times$  assay buffer (Enzo LifeSciences). For this the excitation and emission wavelengths were set to 550 and 600 nm, respectively.

Enzyme activity: We measured the activity of Adk in terms of ADP formation by an end-point assay as described earlier<sup>4</sup>. Briefly, the concentration of AMP was fixed to 500  $\mu\text{M}$  and ATP concentration was varied from 0 to 500  $\mu\text{M}$  in an enzymatic reaction. 5 nM of Adk was used to initiate the reaction and 500  $\mu\text{M}$  of Ap5A was used for quenching at 20, 40, and 60 second time points. The amount of ADP formed was measured by LDH-Pyruvate kinase-coupled reaction and the kinetic parameters were derived by fitting the data to the Michaelis-Menten equation.

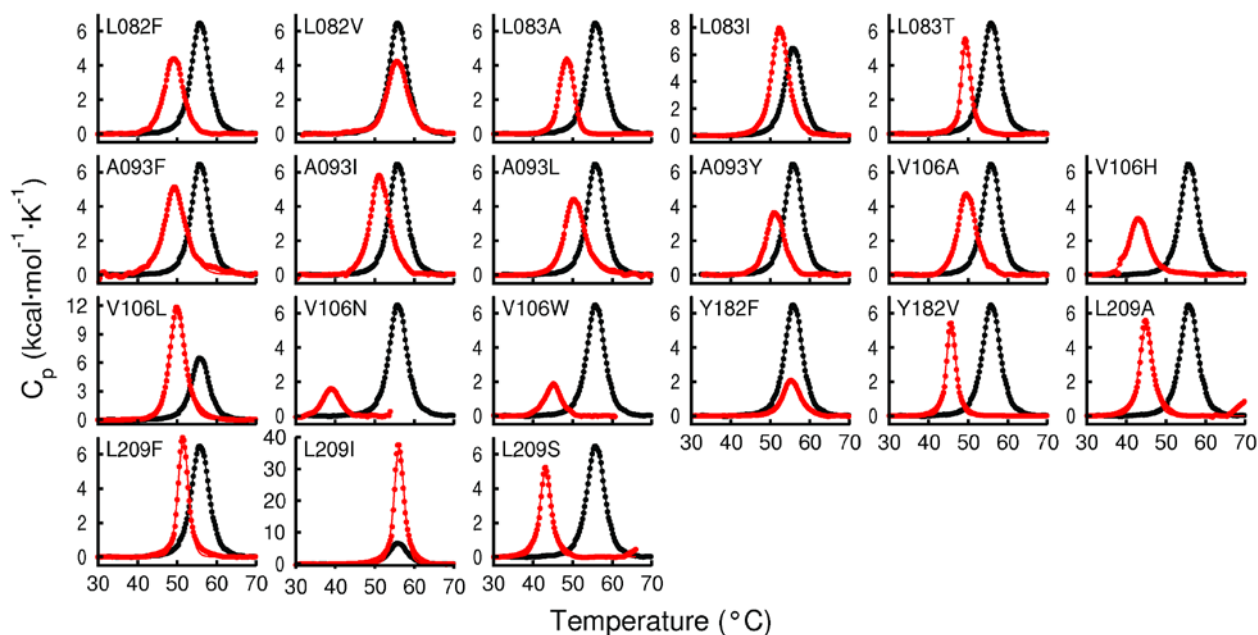
**Adk overexpression:** The *adk* gene was cloned in a pBAD plasmid and transformed in the *E. coli* BW27783 strain (CGSC#12119). This strain constitutively expresses the arabinose transporter (*araE*) which enables uniform uptake of arabinose. The cells were induced with increasing concentrations of arabinose from 0 to 0.05%.

**Intracellular protein abundance:** Cells were grown in supplemented M9 medium for 4 hours at 37 °C, harvested and subsequently lysed with 1× BugBuster (Novagen) and 25 units/ml of Benzonase. Total amount of proteins in cell lysate was estimated by BCA assay. The specific fraction of Adk was determined by SDS-PAGE followed by western blot using rabbit anti-Adk polyclonal antibodies (custom- raised by Pacific Immunology). We used experimentally derived protein abundance values for all analysis reported in this study.

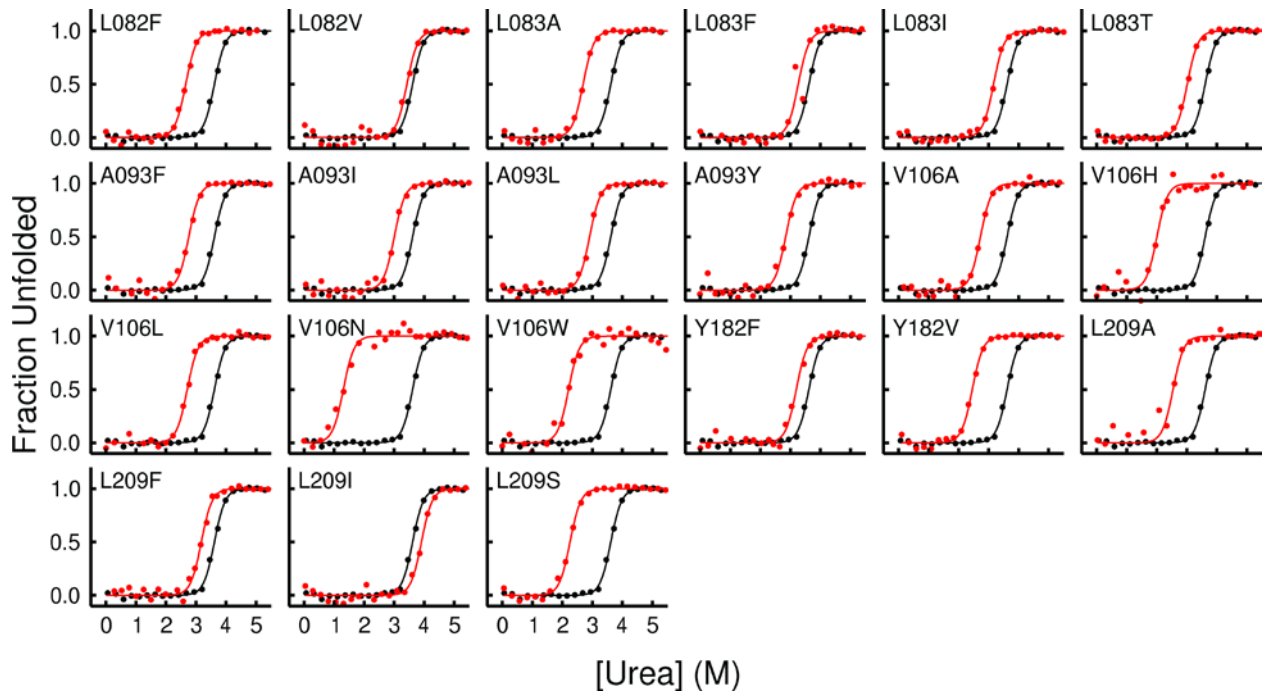
**Estimation of viable cells in saturating culture:** The overnight culture was grown in supplemented M9 medium for 16 hours at 30 °C and the proportion of live:dead cells was measured using Live/Dead BacLight Bacterial Viability Kits (Molecular Probes) according to the manufacturer's instructions. Briefly,  $1 \times 10^8$  cells (in a volume of 1ml) were mixed with 3 µl of a 1:1 proportion of Syto9 dye and Propidium Iodide (PI). The mixture was incubated in the dark for 15 minutes, following which the fluorescence was measured at 530 nm and 630 nm. Syto9 dye stains live cells and emits fluorescence at 530 nm (green), while PI stains dead cells and can be detected at 630 nm (red). The ratio of fluorescence values at 530 nm:630 nm corresponds to the proportion of live:dead cells in that sample which was eventually used to estimate the percentage of live cells in a sample, according to the manufacturer's instructions. An exponentially growing culture (considered as 100% live) and cells treated with 70% ethanol for 1 hour (considered 100% dead) were mixed in different known proportions, and their 530:630 nm ratio was used to generate a standard curve.

**References:**

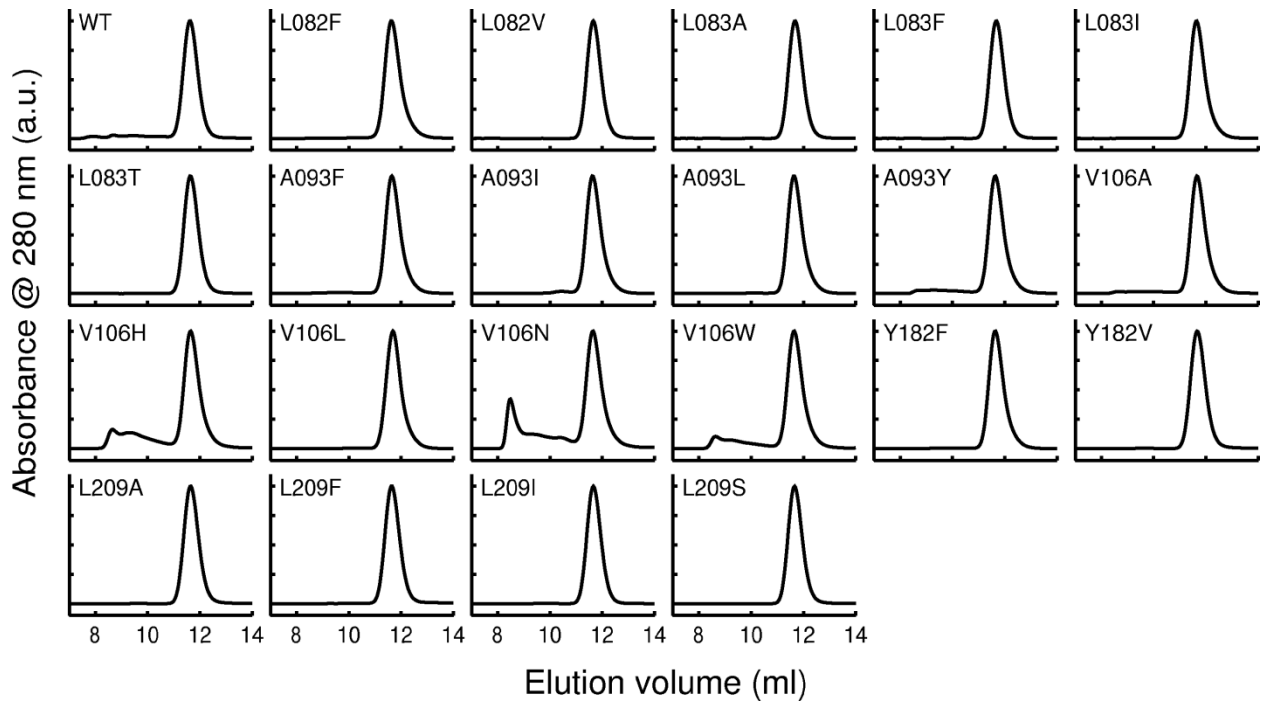
1. Niesen, F.H., Berglund, H. & Vedadi, M. The use of differential scanning fluorimetry to detect ligand interactions that promote protein stability. *Nat Protoc* **2**, 2212-21 (2007).
2. Chen, B.L. & Schellman, J.A. Low-temperature unfolding of a mutant of phage T4 lysozyme. 1. Equilibrium studies. *Biochemistry* **28**, 685-91 (1989).
3. Schellman, J.A. The thermodynamic stability of proteins. *Annu Rev Biophys Biophys Chem* **16**, 115-37 (1987).
4. Pena, M.I., Davlieva, M., Bennett, M.R., Olson, J.S. & Shamoo, Y. Evolutionary fates within a microbial population highlight an essential role for protein folding during natural selection. *Mol Syst Biol* **6**, 387 (2010).



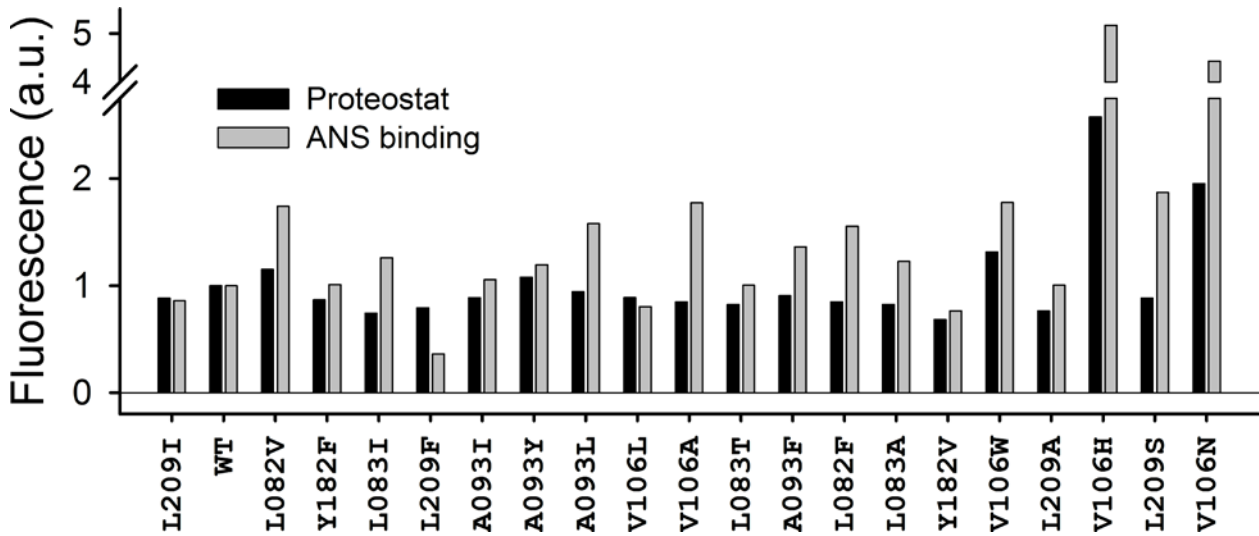
**Supplementary Fig. 1:** Thermal unfolding monitored by Differential Scanning Calorimetry (DSC) for WT (black trace) and 20 different Adk mutant proteins (red trace). The molar heat capacity ( $C_p$ ) is shown as a function of temperature. The scan rate was 90 °C/hr. The data was fitted to a two-state thermal unfolding model to derive the thermodynamic parameters.



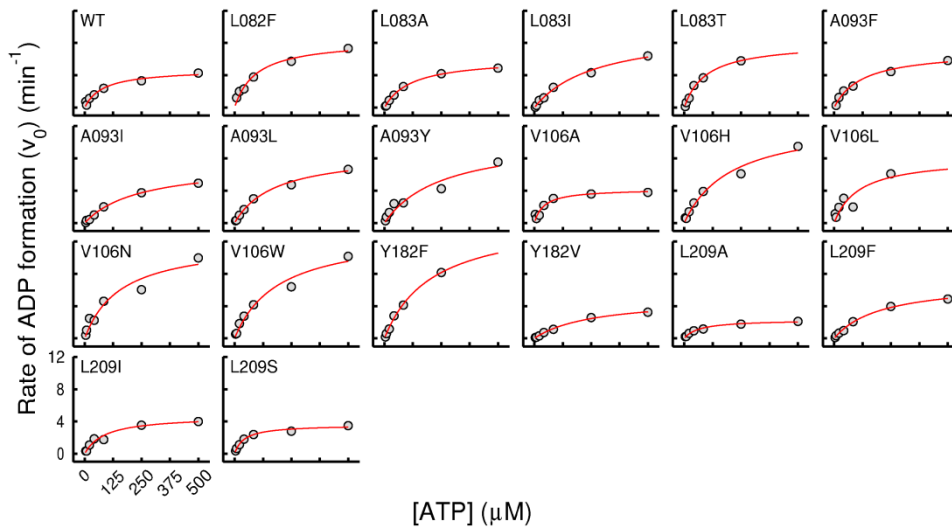
**Supplementary Fig. 2:** Isothermal urea denaturation curves at 25 °C for WT (black dots) and mutant Adk proteins (red dots). The fraction unfolded ( $F_u$ ) is plotted as a function of denaturant concentration. Protein denaturation was monitored by recording the CD signal at 222 nm. The data was fit to a two-state unfolding model.



**Supplementary Fig. 3:** Analytical gel-filtration profile of WT and 20 mutant Adk proteins on a Superdex-75 column at room-temperature. The absorbance at 280 nm is shown as a function of elution volume. For comparison all the monomeric peaks were normalized to 1. WT Adk along with most other mutant proteins elutes at the expected position for a monomer. Exceptions were V106H, V106N and V106W, where additional peaks appear at much higher molecular weights.

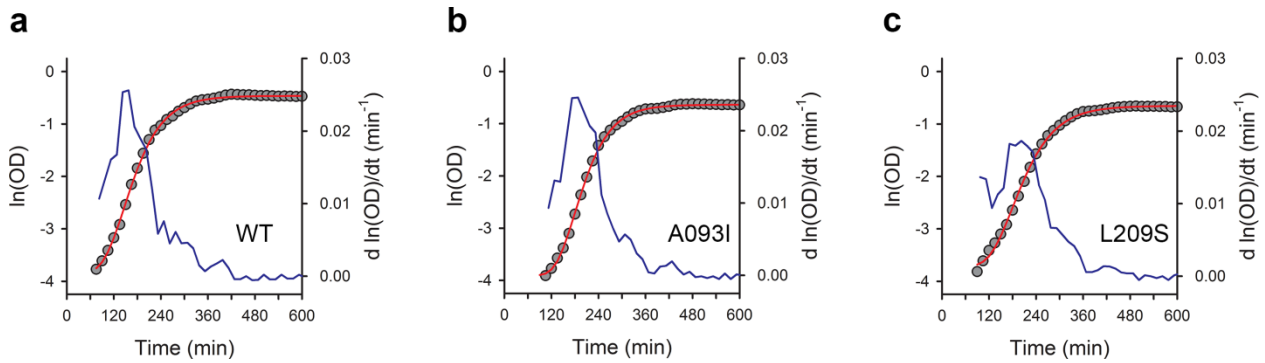


**Supplementary Fig. 4:** Aggregation propensity and molten-globule states of mutant proteins. Bar plots represent the extent of ProteoStat and ANS binding to WT and mutant Adk proteins. The proteins on the x-axis are arranged in decreasing order of stability from left to right.

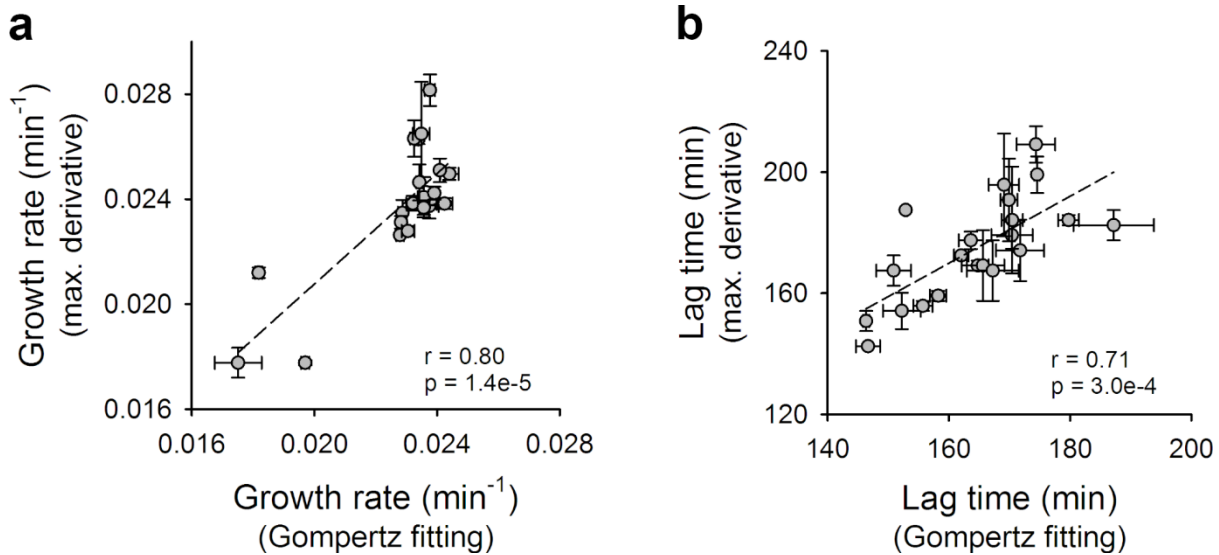


**Supplementary Fig. 5:** Enzyme activity of Adk mutants at 25 °C measured as described in Supplementary methods. The initial velocity, shown as a function of ATP concentration, was calculated as the amount of ADP produced per minute by 1 nmol of Adenylate Kinase. The concentration of AMP in all experiments was fixed to 500  $\mu\text{M}$ . The data (gray circles) was fitted using the Michaelis-Menten equation of enzyme activity to extract relevant parameters (fitted line in red).

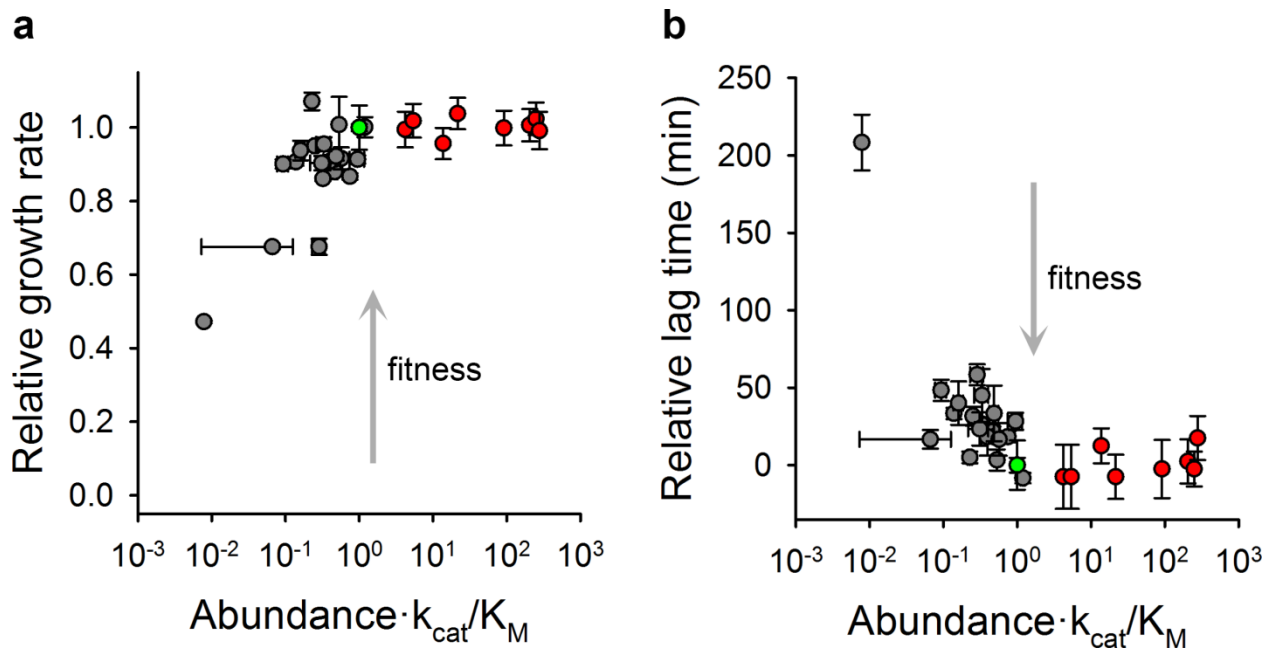




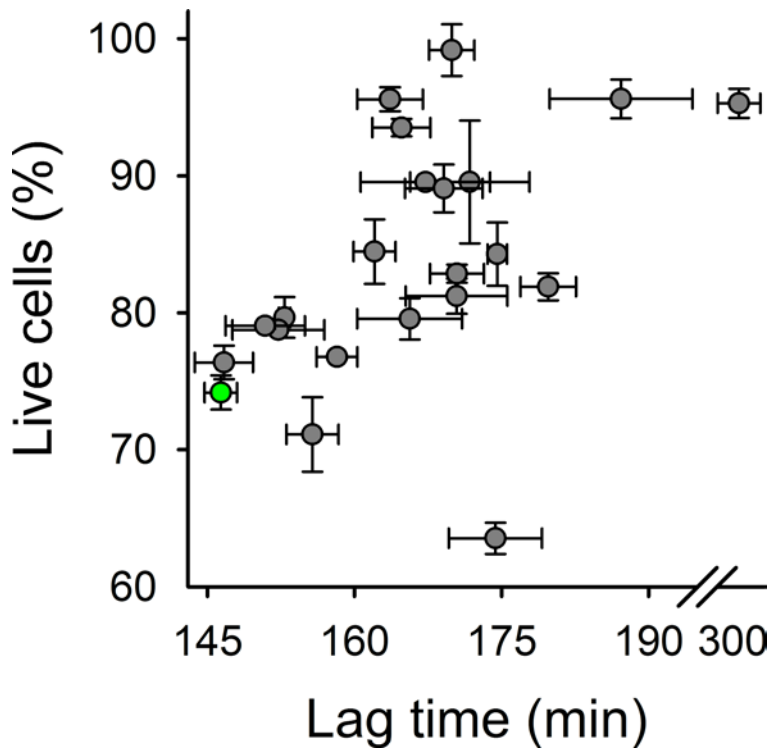
**Supplementary Fig. 6:** Representative growth curves of (a) WT, (b) A093I, and (c) L209S strains. Each growth curve is shown as  $\ln(\text{OD})$  vs time plot (left y-axis). The experimental data is shown in gray circles and the Gompertz fit is shown in solid red line. The instantaneous time derivative of the  $\ln(\text{OD})$  data is shown in blue line (right y-axis). The strains were chosen to illustrate the quality of the fit across different range of growth rates and lag times (see Supplementary Table 2 for growth parameters).



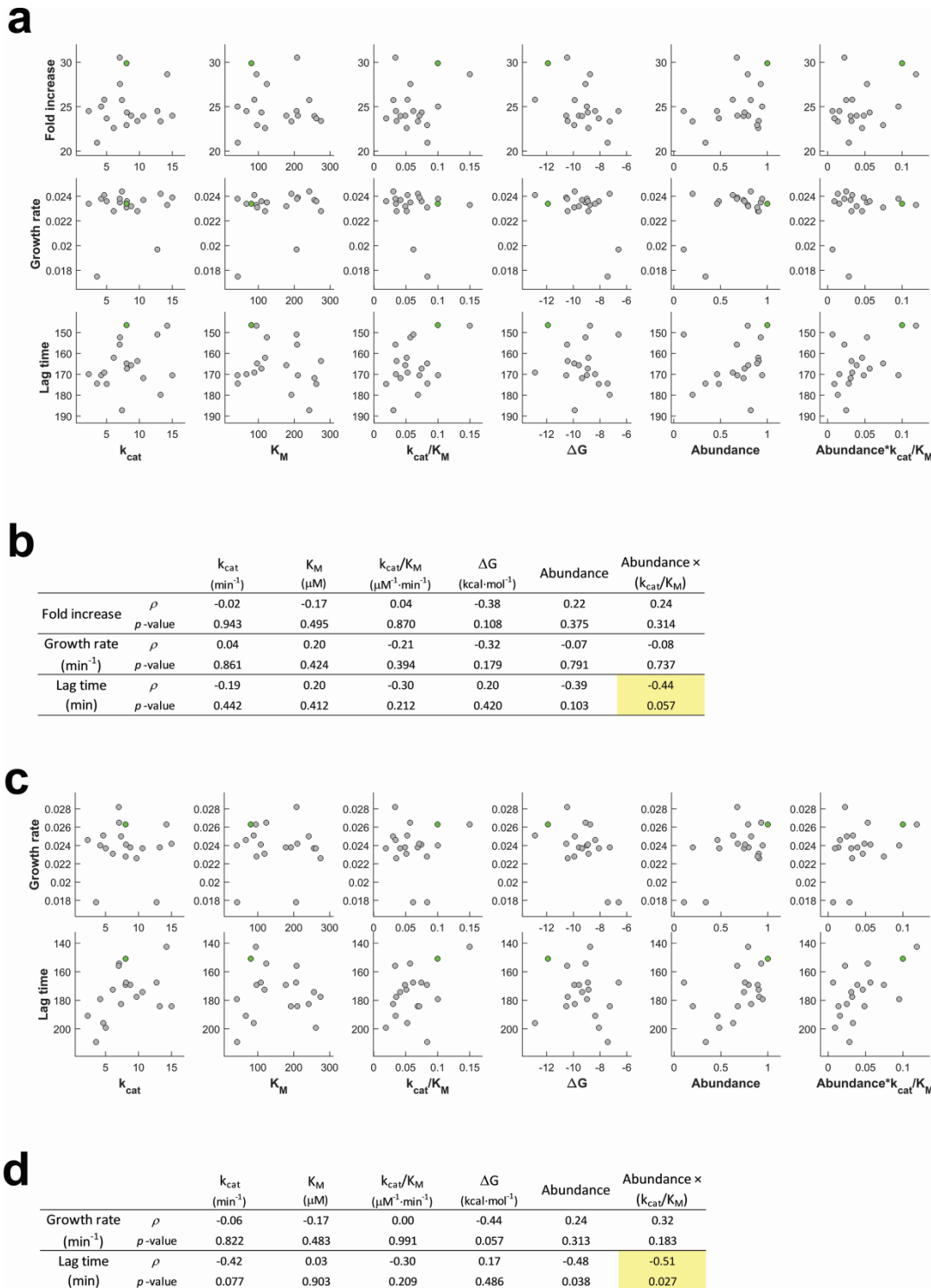
**Supplementary Fig. 7:** Correlation between growth parameters derived from Gompertz fitting and maximum-derivative method (a,b). The parameters derived from both the methods correlate very well as indicated by Pearson’s correlation parameters ( $r$  and  $p$ -values). The data points represent mean and error bars are s.e.m. of parameters derived from 2-3 bacterial colonies (see Supplementary Table 2).



**Supplementary Fig. 8:** Traits of population growth. (a) Relative growth rates ( $\mu/\mu_{WT}$ ) and (b) relative lag time ( $\lambda - \lambda_{WT}$ ) obtained from analysis of growth curve derivatives shown as a function of catalytic capacity which is defined as  $\text{abundance} \times k_{cat}/K_M$ . The mutant data is shown in gray circles, whereas red circles represent the BW27783 strain with varying degrees of overexpression of WT Adk from a pBAD plasmid. Data for WT is shown in green. The data points are mean and error bars are s.e.m. of parameters derived from 2-3 bacterial colonies (see Supplementary Table 2). Fig 2 is an equivalent figure with growth rate and lag times obtained after fitting the raw data with Gompertz equation (equation (2)).

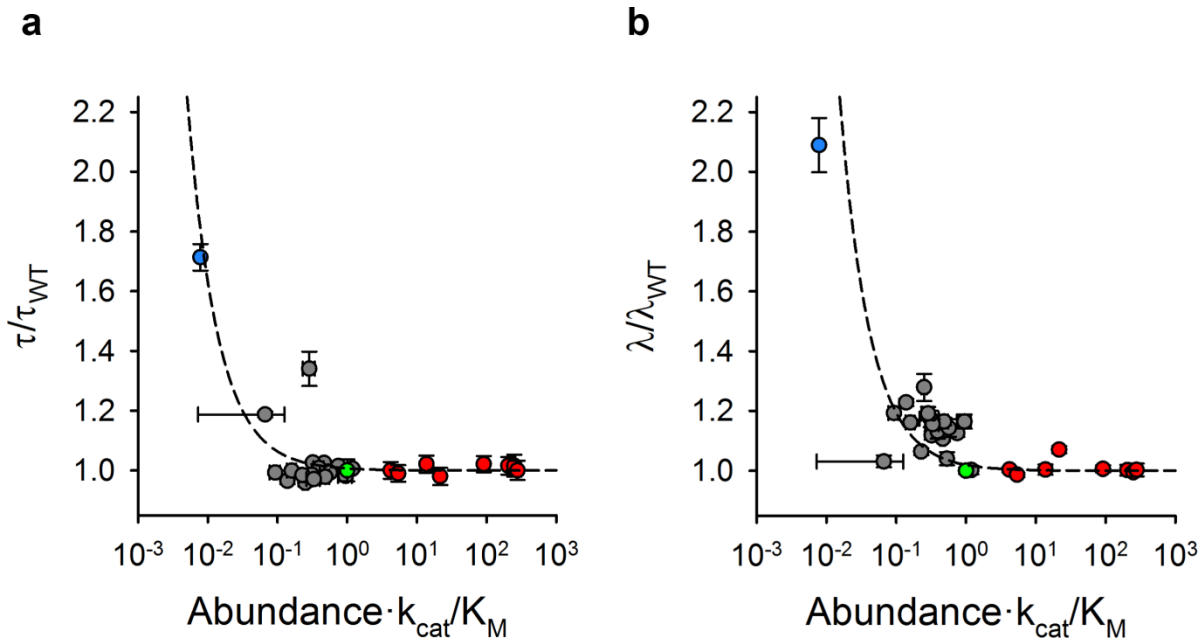


**Supplementary Fig. 9:** Percentage of live or viable cells of WT and mutant Adk strains at saturation (16 hours of growth) versus their population lag time. The cultures were grown overnight at 30 °C, and then stained using fluorescent dyes Syto9 (specific for live cells) and propidium iodide (specific for dead cells). The data points are mean and error bars represent standard deviation of 2 biological replicates. WT Adk strain is shown in green.

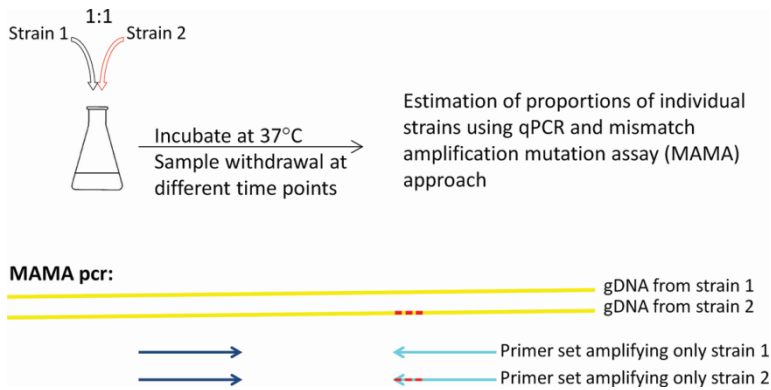


**Supplementary Fig. 10:** Scatter plots of growth parameters (carrying capacity, growth rate and lag times) and molecular and cellular properties of Adk. Parameters were obtained using (a) Gompertz fit and (c) analysis of growth curve derivatives. Panels (b) and (d) show Spearman's correlation coefficients ( $\rho$ ) and  $p$ -values for each of the sub-plots in panels (a) and (c)

respectively. The highest correlation values in each panel are highlighted in yellow. V106N was excluded from all correlation calculations.



**Supplementary Fig. 11:** (a) Relative growth time ( $\tau/\tau_{WT}$ ) and (b) relative lag time ( $\lambda/\lambda_{WT}$ ) as a function of catalytic capacity ( $\text{abundance} \times k_{cat}/K_M$ ). The dashed line shows a fit to Eq. 3, where the asymptote ( $a$ ) was assumed to be 1. The  $K_M$ -like parameter  $b$  for growth time was 0.006 and that for lag time was 0.019, which indicates that the WT catalytic capacity is closer to the cusp for lag time than for growth time. The mutant data is shown in gray circles, whereas the overexpression data is shown in red. In green is shown WT, while the blue circle indicates V106N which was omitted from the fitting. The error bars represent s.e.m. of parameters derived from growth curves of 2-3 bacterial colonies (biological replicates). See Supplementary Tables 2 and 3 for the parameters.



**Supplementary Fig. 12:** Schematic representation of binary growth competition experiments and estimation of relative proportion of competing strains. The strains (1) and (2) are mixed in 1:1 proportion and were grown at 37 °C. Samples were drawn at different time points, normalized for OD, and genomic DNA was extracted. The proportions of individual strains were estimated by a qPCR method employing mismatch amplification mutation assay method (see Methods). We designed a set of primers to differentially amplify the strains by matching the 3'-end of one of the primers to the site of mutation and using Taq DNA polymerase for amplification.



Supplementary Table 1: Structural and biophysical parameters

adk strain	SC acc <sup>a</sup> (%)	Residue depth (Å)	Fraction of WT in MSA	Fraction of mutant in MSA <sup>b</sup>	T <sub>m</sub> (DSC) (°C)	T <sub>m</sub> (TFA) <sup>c</sup> (°C)	ΔG <sup>d</sup> (kcal/mol)	k <sub>cat</sub> <sup>e</sup> (min <sup>-1</sup> )	K <sub>M</sub> <sup>f</sup> (μM)	k <sub>cat</sub> /K <sub>M</sub> (μM <sup>-1</sup> min <sup>-1</sup> )
WT	--	--	--	--	55.9	53.8	-11.9	8.05	80.58	9.99E-02
L082F	0.0	8.8	0.57	0.00	49.2	47.4	-8.7	14.23	94.86	1.50E-01
L082V	0.0	8.8	0.57	0.14	55.7	53.2	-11.3	n.d. <sup>g</sup>	n.d. <sup>g</sup>	n.d. <sup>g</sup>
L083A	0.1	9.0	0.70	0.00	48.5	46.9	-8.9	6.10	118.73	5.13E-02
L083F	0.1	9.0	0.70	0.60	n.d. <sup>g</sup>	54.2	-10.8	n.d. <sup>g</sup>	n.d. <sup>g</sup>	n.d. <sup>g</sup>
L083I	0.1	9.0	0.70	0.23	52.4	50.7	-10.4	9.70	274.80	3.53E-02
L083T	0.1	9.0	0.70	0.00	49.4	49.3	-9.9	8.05	96.55	8.34E-02
A093F	0.0	5.9	0.85	0.00	49.4	47.2	-9.1	7.05	123.83	5.69E-02
A093I	0.0	5.9	0.85	0.00	51.3	49.7	-9.9	7.34	241.75	3.04E-02
A093L	0.0	5.9	0.85	0.07	50.6	47.9	-9.6	8.75	178.05	4.91E-02
A093Y	0.0	5.9	0.85	0.00	51.2	49.4	-9.3	10.61	256.23	4.14E-02
V106A	0.0	7.4	0.74	0.38	49.7	47.3	-9.0	4.19	41.78	1.00E-01
V106H	0.0	7.4	0.74	0.00	43.2	41.2	-6.6	12.74	206.54	6.17E-02
V106L	0.0	7.4	0.74	0.04	50.1	48.5	-8.9	8.10	108.60	7.46E-02
V106N	0.0	7.4	0.74	0.00	39.0	37.9	-4.8	12.07	158.06	7.64E-02
V106W	0.0	7.4	0.74	0.04	45.0	43.0	-7.3	13.22	192.05	6.88E-02
Y182F	7.2	6.3	0.86	0.14	55.4	53.8	-10.5	15.00	210.25	7.13E-02
Y182V	7.2	6.3	0.86	0.00	45.7	46.2	-8.1	5.01	261.53	1.92E-02
L209A	0.0	7.0	0.23	0.08	45.0	44.3	-8.4	2.30	66.94	3.43E-02
L209F	0.0	7.0	0.23	0.01	51.5	51.0	-10.5	7.00	208.17	3.36E-02
L209I <sup>h</sup>	0.0	7.0	0.23	0.58	56.1	55.5	-12.9	4.66	88.82	5.25E-02
L209S	0.0	7.0	0.23	0.00	43.2	42.4	-7.4	3.57	42.55	8.38E-02

<sup>a</sup> % sidechain accessibility calculated using coordinates of pdb 4ake

<sup>b</sup> fraction in multiple sequence alignment when WT amino acid is excluded

<sup>c</sup> melting temperature from thermofluor assay

<sup>d</sup> derived from isothermal urea denaturation experiments at 25C

<sup>e</sup> kcat for ADP formation

<sup>f</sup> KM for ATP

<sup>g</sup> not determined

<sup>h</sup> the only case in this dataset where fraction of mutant amino acid was greater than WT amino acid in MSA

**Supplementary Table 2: Intracellular abundance and growth parameters of adk mutants**

Adk strain	Fold-increase, $K^a$	error in $K^b$	Growth rate, $\mu^a$ ( $\text{min}^{-1}$ )	error in $\mu^b$	Lag time, $\lambda^{a,c}$ (min)	error in $\lambda^b$	Abundance <sup>d</sup>	error in abundance <sup>e</sup>
WT	30.0	1.3	0.0234	1.09E-04	146.4	0.5	1.00	0.00
L082F	28.8	1.8	0.0233	1.39E-04	146.7	2.0	0.79	0.05
L082V	24.4	0.4	0.0229	1.45E-04	158.2	1.3	n.d. <sup>f</sup>	n.d. <sup>f</sup>
L083A	22.6	0.4	0.0228	9.49E-05	162.0	1.2	0.90	0.08
L083F <sup>g</sup>	27.3	1.0	0.0182	1.17E-04	152.9	0.2	1.19	0.10
L083I	23.4	0.3	0.0228	1.25E-04	163.6	2.0	0.91	0.02
L083T	22.9	0.1	0.0231	2.12E-04	164.8	1.8	0.89	0.03
A093F	27.8	2.7	0.0235	2.75E-04	152.2	3.1	0.93	0.03
A093I <sup>g</sup>	25.8	0.2	0.0244	3.00E-04	187.2	6.6	0.82	0.07
A093L	24.0	0.5	0.0232	2.12E-04	165.6	3.5	0.80	0.13
A093Y	24.0	0.4	0.0237	3.08E-04	171.7	4.0	0.75	0.23
V106A	25.0	0.1	0.0238	1.95E-04	170.4	3.4	0.95	0.21
V106H <sup>g</sup>	24.6	1.3	0.0197	1.33E-04	150.9	2.9	0.11	0.10
V106L	24.4	1.1	0.0236	1.95E-04	167.2	4.3	0.76	0.05
V106N	5.9	0.1	0.0137	3.62E-04	305.8	13.2	0.01	0.00
V106W	23.4	0.6	0.0242	2.61E-04	179.7	1.7	0.20	0.01
Y182F	24.0	0.5	0.0239	1.06E-04	170.4	1.8	0.68	0.09
Y182V	23.7	0.6	0.0236	1.39E-04	174.6	0.5	0.48	0.08
L209A	24.5	0.4	0.0234	1.06E-04	169.9	1.4	0.46	0.07
L209F	30.6	0.7	0.0238	1.64E-04	155.7	1.6	0.68	0.05
L209I	25.8	0.7	0.0241	4.84E-05	169.1	2.5	0.63	0.14
L209S	21.0	0.9	0.0175	7.67E-04	174.4	3.2	0.34	0.07

<sup>a</sup> parameters derived by fitting Gompertz equation (equation (2)) to ln(OD) vs time at 37 C<sup>b</sup> SEM derived from 3 bacterial colonies (biological replicates)<sup>c</sup> time required to achieve maximum growth rate<sup>d</sup> abundance measured after 4h of growth at 37 C<sup>e</sup> standard deviation derived from 2 bacterial colonies (biological replicates)<sup>f</sup> not determined<sup>g</sup> growth parameters derived from 2 bacterial colonies (biological replicates)

**Supplementary Table 3: Intracellular abundance and growth parameters of WT *adk* overexpression from pBAD plasmid in *E. coli* BW27783 strain**

arabinose concentration (%)	Carrying capacity, $K^a$	s.d. in $K^b$	Growth rate, $\mu^a$ ( $\text{min}^{-1}$ )	s.d. in $\mu^b$	Lag time, $\lambda^{a,c}$ (min)	s.d. in $\lambda^b$	Abundance <sup>d</sup>	s.d. in abundance <sup>e</sup>
no plasmid	29.5	2.5	0.0195	5.10E-04	126.7	1.0	1.00	0.10
0.00E+00	32.0	0.5	0.0195	2.00E-04	127.2	0.7	4.20	0.42
3.05E-06	30.9	1.8	0.0191	2.00E-04	127.2	2.0	13.73	1.37
1.22E-05	31.3	1.0	0.0197	2.00E-04	125.0	0.4	5.39	0.54
4.88E-05	27.1	1.0	0.0199	2.65E-04	135.7	1.1	21.55	2.15
1.95E-04	32.7	0.9	0.0191	1.00E-04	127.5	1.2	91.27	9.12
7.81E-04	31.6	2.5	0.0192	2.52E-04	127.0	2.1	205.31	20.51
3.13E-03	32.6	1.6	0.0192	4.73E-04	126.1	1.4	250.39	25.02
5.00E-02	28.4	3.1	0.0195	3.61E-04	127.1	2.5	278.69	27.84

<sup>a</sup> parameters derived by fitting Gompertz equation (equation (2)) to  $\ln(\text{OD})$  vs time at 37 C

<sup>b</sup> standard deviation of 3 replicates (from single bacterial colony)

<sup>c</sup> time required to achieve maximum growth rate

<sup>d</sup> abundance measured after 4h of growth at 37 C

<sup>e</sup> standard deviation derived from 2 bacterial colonies (biological replicates)